JOURNAL OF GEOPHYSICAL RESEARCH, VOL. 111, D23202, doi:10.1029/2006JD007273, 2006

Impact of clouds on radiative heating rates in the tropical lower stratosphere

S. Fueglistaler[1] and Q. Fu[1]

Received 8 March 2006; revised 4 August 2006; accepted 18 August 2006; published 5 December 2006.

[1] We quantify the impact of tropospheric clouds on radiative heating rates in the tropical lower stratosphere using the data collected from the Atmospheric Radiation Measurement (ARM) Tropical Western Pacific (TWP) sites Manus and Nauru. The cloud fields are retrieved from ground-based millimeter cloud radar observations. We find that the radiative heating rate change due to enhanced upwelling shortwave fluxes only partially compensates that due to reduced upwelling longwave fluxes, resulting in a net change of about −0.2 K/day in the 70–30 hPa layer during the periods of frequent high cloud occurrence. The impact of clouds is particularly large relative to clear sky radiative heating rates around 60 hPa (435–475 K, the base of the "tropical pipe") where they show a local minimum. The radiative heating rates in this layer with the consideration of cloud effects are close to zero and can be even negative (i.e., diabatic descent). The seasonal and spatial structures of tropical convection, and associated high cloud coverage, suggest that their effect, leading to longitudinal (in addition to the well known latitudinal) gradients in radiative heating rates, may be partially responsible for stratospheric mixing. It is suggested that the effect of high tropospheric clouds on radiative heating rates cannot fully explain the amplitude of diabatic descent in the lower stratosphere over the maritime continent reported in previous studies.

Citation: Fueglistaler, S., and Q. Fu (2006), Impact of clouds on radiative heating rates in the tropical lower stratosphere, *J. Geophys. Res.*, *111*, D23202, doi:10.1029/2006JD007273.

1. Introduction

[2] The wave-driven stratospheric Brewer-Dobson circulation forces an upwelling over the tropics that is balanced by radiative heating [*Holton et al.*, 1995]. The heating rates and upwelling show substantial spatial and temporal variability, with enhanced upwelling at the edges of the tropics [e.g., *Eluszkiewicz et al.*, 1997; *Plumb and Eluszkiewickz*, 1999]. Estimates of radiative heating rates [e.g., *Rosenlof*, 1995] provide important information about the mechanisms of tropical upwelling. The radiative heating rates derived from radiative transfer calculations are, among others, sensitive to ozone concentrations, temperatures, and tropospheric cloud fields. *Sherwood* [2000] analyzed operational wind data over the Maritime continent area and found, in order to close the energy budget over this region, a need for an energy sink equivalent to a cooling of about 1.5 K/day, which was hypothesized to be arising from mixing with overshooting convection. *Hartmann et al.* [2001b] discussed the role of thin cirrus clouds overlaying thick anvil clouds, which could lead to local (in the cloud layer) radiative cooling, as an alternative to overshooting convection. *Norton* [2001] noted a strong anticorrelation between upper tropospheric cloud cover and lower stratospheric heating rates in ECMWF data, which was interpreted as a possible consequence of the reduced longwave heating in the lower stratosphere in the presence of high clouds. Descent over the tropical Western Pacific region was also noted in the vertical wind fields of assimilated data by *Simmons et al.* [1999] and *Gettelman et al.* [2000].

[3] The map of diabatic heating (in terms of potential temperature) at 70 hPa shown by *Norton* [2001] indicates a spatial variation of about 1.5 K/day near the equator, with diabatic heating rates ranging from less than −0.3 K/day over the maritime continent to larger than 1.2 K/day over the eastern Pacific. *Fueglistaler et al.* [2004] studied the diabatic motion with trajectory calculations based on ECMWF wind fields and obtained similar patterns, in particular a region of diabatic descent over the maritime continent. Their analysis of the three-dimensional structure showed diabatic descent from tropopause levels upward, with diabatic descent of order a few Kelvin in potential temperature per day.

[4] Here, we present calculations of radiative heating rates where we specifically pay attention to an accurate representation of clouds in order to better quantify their role, and hence to allow for better constraining the processes that affect the diabatic circulation of the tropical lower stratosphere. Clouds affect stratospheric heating rates in a number of ways, depending on time of day, and altitude of cloud. Briefly, the increased albedo in the presence of clouds leads to an increase in reflected, upwelling shortwave radiation.

[1]Department of Atmospheric Sciences, University of Washington, Seattle, Washington, USA.

0148-0227/06/2006JD007273$09.00

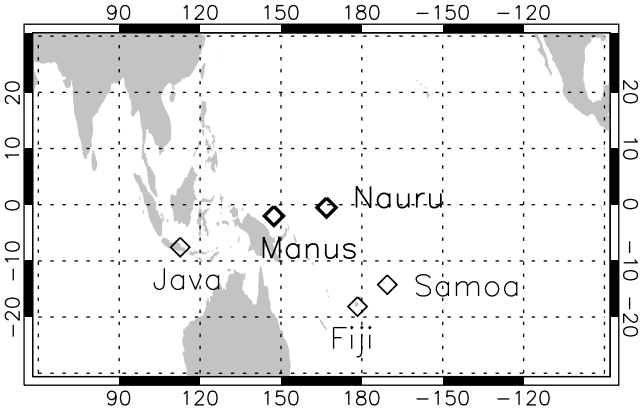

Figure 1. Location of the ARM stations Manus and Nauru (bold) and the SHADOZ stations Java, Fiji, and Samoa.

This effect leads to an increase in stratospheric heating rates, and is not sensitive to the altitude of the cloud (the shortwave absorption in the troposphere is small), but, obviously, depends on the cloud optical depth and time of day. Conversely, clouds reduce the upwelling longwave radiation which leads to a reduction of stratospheric heating rates, mainly due to a reduction in absorption at the 9.6 μm ozone band. This effect is independent of the time of day, but depends on optical depth and the altitude of the clouds (due to the cloud's emission temperature). The low effective emission temperature associated with high thick clouds has strong impact on the outgoing longwave radiation. Conversely, low clouds have little impact because of small difference between the cloud and surface temperatures.

[5] A number of studies have estimated the impact of tropospheric clouds, typically with idealized cloud fields [e.g., *Eluszkiewicz et al.*, 1997; *Hicke and Tuck*, 1999; *Hartmann et al.*, 2001b; *Gettelman et al.*, 2004]. *Corti et al.* [2005] used the observations of tropical thin cirrus and cloud top height during 10–19 September 1994 provided by the Lidar-In Space Technology Experiment (LITE) to complement cloud information provided by the International Satellite Cloud Climatology Project (ISCCP) to calculate radiative heating rates. A careful analysis of the effect of clouds on stratospheric heating rates is warranted, using an accurate description of the cloud field in terms of occurrence frequency (on annual, seasonal and diurnal timescales), cloud altitudes and optical depths.

[6] Here, we derive the cloud characteristics from the Millimeter cloud radar (MMCR) observations of the ARM sites Manus and Nauru. This allows an accurate description of the cloud field with respect to altitude, optical depth, frequency of occurrence, and diurnal and seasonal variability. The two sites are located in the western Pacific warm pool, with frequent deep convection, and a very high cloud occurrence frequency for high clouds [e.g., *Hartmann et al.*, 2001a]. Hence we may derive from data of this region an upper bound of the impact of clouds, with a smaller role of clouds in the zonal mean radiative heating rates. Note that the cloud retrieval based on MMCR data underestimates some high, thin cirrus clouds, and we will also discuss its implications to our conclusions.

2. Data and Method

[7] We use data from the ARM stations Manus and Nauru, complemented with ozone data from the Southern Hemisphere Additional Ozone soundings (SHADOZ) program [*Thompson et al.*, 2003] stations Java, Fiji and Samoa (locations shown in Figure 1). Data from the years 2000 (a weak La Nina year) and 2002 (a weak El Nino situation that is developing over the course of the year) are used to calculate radiative heating rates around the tropopause and in the lower stratosphere over the sites Manus and Nauru. Results of the radiative transfer calculations will be shown in general from the upper troposphere upward. However, we emphasize here the results from the tropopause (about 380 K, equivalent to ~90 hPa, or 17 km) upward, as heating rates in the tropical tropopause layer (TTL, loosely defined as the layer between the level of zero net radiative heating and the tropopause) may be affected by the presence of thin cirrus, which may go undetected by the radar system used for the cloud retrieval. (A discussion of the sensitivity of our calculations to these thin cirrus clouds is given in section 3.5.)

[8] Radiative heating rates reported in this paper are always in terms of temperature change per day (as opposed to changes in potential temperature, θ). Assuming reversible adiabatic expansion/contraction, these heating rates may be converted to changes in potential temperature (θ) using the expression:

$$\partial\theta/\partial t = \partial T/\partial t \cdot (p/1000)^{-2/7}$$

where t is time, p is pressure (in hPa) and T is temperature. In the pressure range of interest here, $(p/1000)^{-2/7}$ = 1.72,1.93 and 2.35 for p = 150, 100 and 50 hPa, respectively.

2.1. Data

[9] We use the temperature and water vapor (rawinsonde) measurements from the ARM TWP sites of the years 2000 (Manus) and 2000/2002 (Nauru), when sufficient data are available. These soundings are typically launched once or twice a day, and reach well into the stratosphere with altitudes higher than 30 hPa (about 24 km). The temperature profiles are extended in the vertical using UKMO stratospheric analysis data. Hence the results of the radiative transfer calculations in the region of interest here, namely from the upper troposphere up to about 30 hPa are based on the sonde temperatures, whereas higher up the results are increasingly dominated by the UKMO temperature profiles. To make use of the higher sampling rate (in time) of surface temperature measurements at the ARM sites, the temperature profiles are interpolated in time with consideration of these surface measurements, whereby the surface variations are vertically extrapolated up to the upper troposphere, with the weights decaying with height. Water vapor measurements from radiosondes are known to be unreliable in the upper troposphere, and suffer from a dry bias [*Wang et al.*, 2003; *Miloshevich et al.*, 2004]. We have evaluated the sensitivity of the radiative transfer calculations to changes in

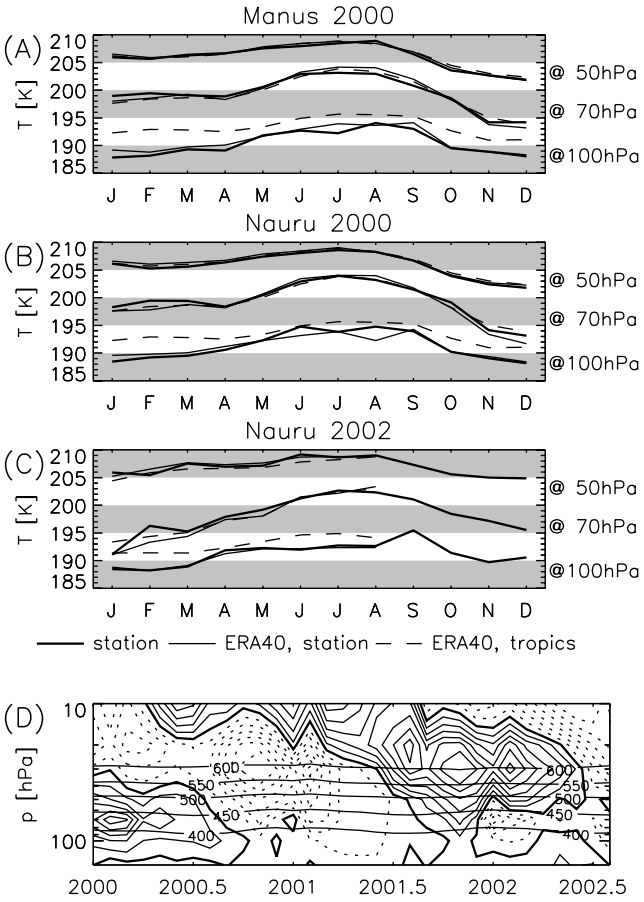

Figure 2. Monthly mean temperatures at pressure levels of 100, 70, and 50 hPa at (a) Manus in 2000, (b) Nauru in 2000, and (c) Nauru in 2002. Bold solid lines are temperatures based on rawinsonde measurements at Manus and Nauru (used for all calculations shown here). For comparison, the thin lines show ERA-40 temperatures, where the solid line is at the location of the station and the dashed line is the tropical mean (zonally averaged, from 10°S to 10°N). (d) Temperature anomalies of tropical mean temperatures after subtracting the mean annual cycle of this period. Contour line spacing is 0.5 K, dashed lines show negative anomalies, bold line is zero, and solid lines are positive anomalies. Thin horizontal lines show isentropes between 400 and 600 K. Temperature anomalies are induced by the QBO, westerly wind shear corresponds to positive anomalies. Note that ERA-40 data end August 2002.

water vapor concentrations in the pressure range of 300–100 hPa. We find that absolute radiative heating rates in that layer are sensitive to changes, a point we will further discuss below. However, heating rates in the stratosphere are only marginally different even when water vapor concentrations in this layer were increased by 20%. More important, the difference in stratospheric radiative heating rates between all sky and clear sky calculations, the main focus of this paper, are barely affected by changes of order 20% in upper tropospheric water vapor concentrations. Water vapor concentrations in the stratosphere are set to typical values (4.5 ppmv, results are not sensitive to this value).

[10] Figure 2 shows the monthly mean temperatures (bold lines) at 100, 70 and 50 hPa for Manus in 2000, and for Nauru in 2000 and 2002. Figure 2 further shows the monthly mean temperatures of the ECMWF reanalysis project ERA-40 [*Simmons and Gibson*, 2000] for comparison (note that ERA-40 data end in August 2002). The monthly mean temperatures at the grid positions near Manus and Nauru (thin solid lines) agree well with those based on the ARM sondes. The temperatures show the typical seasonal variability of the lower stratosphere. The comparison with the tropical zonal mean (averaged from 10°S to 10°N) temperatures (thin dashed lines) shows that the temperatures near the tropopause over the western Pacific are substantially lower (about 4 K) than those of the tropical mean, whereas those of the lower stratosphere are close to the tropical mean. Figure 2d shows the deseasonalized tropical mean temperature anomalies, mainly induced by the stratospheric Quasi Biennial Oscillation (QBO). In the region of interest here (up to about 30 hPa, or 600 K potential temperature), the zonal mean temperatures decrease by about 2 to 3 K during the year 2000. In 2002, high temperature anomalies persist at higher levels until about May. Note that the QBO-induced temperature anomalies in the lower stratosphere are about a factor 2 smaller than those of the seasonal cycle.

[11] Cloud information is retrieved from the ARM millimeter cloud radar (MMCR; [*Moran et al.*, 1998]). The availability of valid MMCR data is shown in Figure 3, with the percentage of observations of each month resolved by time of day (as previously discussed, cloud effects depend

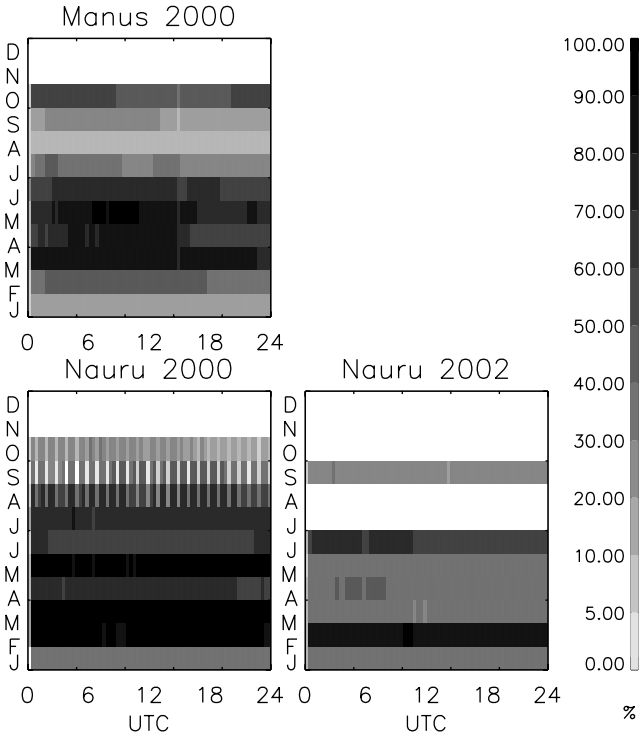

Figure 3. Data availability for Manus 2000, Nauru 2000 and Nauru 2002. Grey scale shows percentage of the observational data available as a function of the time of the day for each month. The sampling period used for the radiative transfer calculations is 20 min.

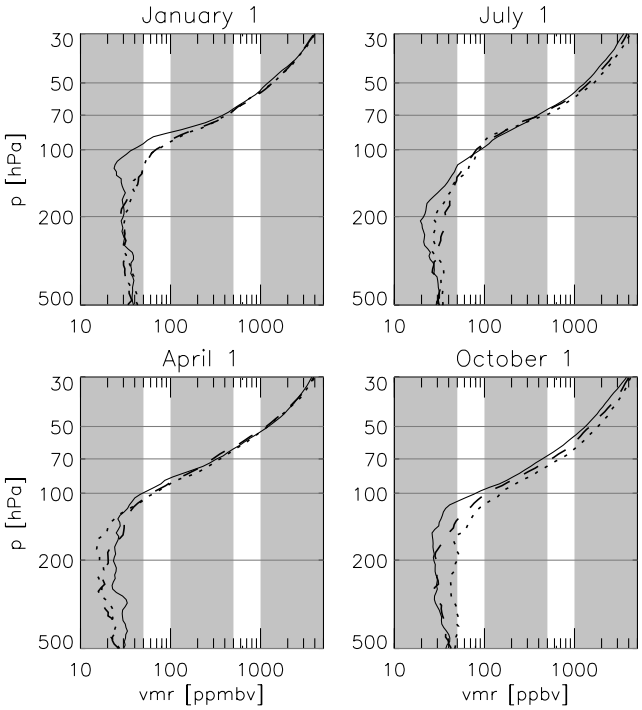

Figure 4. Ozone profiles from the SHADOZ stations Java (solid), Fiji (dashed) and Samoa (dotted). Data are climatological mean annual cycle obtained from fitting with harmonics of periods 12, 6, and 27/12 months (27/12 months to account for QBO-related variations) to the observed profiles in the period 1998–2004.

on solar insolation, and hence great care has to be taken to avoid biases arising from sampling biases). Figure 3 shows that in the year 2000 there are no data for both stations in November and December. In 2002, not enough data are available for Manus, such that only data from Nauru are used, where data for 7 months are available. Moreover, for some months there is valid information available for less than a third of the month only, and occasionally the sampling frequency is quite irregular with respect to time of day. We mitigate the problems arising from this irregular sampling by carefully constructing monthly mean diurnal cycles for each month; that is, all data within a given month are first binned and averaged according to their UTC, and subsequently averaged for the monthly mean. (Note that the radiative transfer calculations (see section 2.3) are performed for individual cloud profiles before such binning.)

[12] Unfortunately, the ARM sites do not provide ozone measurements. Ozone is very important for the absorption and emission in the area of interest [e.g., *Doherty et al.*, 1984; *Gettelman et al.*, 2004]. Accurate ozone profiles are further required because ozone concentrations show a steep vertical gradient, and a small misplacement in the vertical strongly affects the resulting radiative heating rate profile. The lack of colocated ozone concentration measurements is a caveat particularly for the calculation of the (absolute) heating rates in the lower stratosphere. However, the effect of clouds on the heating rates (being the difference between two calculations that assume the same ozone profile), is much less sensitive to uncertainty in ozone mixing ratios (see below).

[13] We therefore use ozone measurements from the SHADOZ network. SHADOZ stations near Manus and Nauru are Java, Fiji and Samoa (see Figure 1). Figure 4 shows the climatological mean (obtained from data spanning 1998–2004) seasonal ozone concentration profiles for these stations. Figure 4 not only shows substantial variability over the course of the year, but also substantial differences between the stations, with the measurements over Java being typically at the lower end. The conditions over Java, being close to the equator with frequent deep convection, may be similar to those over Manus and Nauru, such that these observations were selected as the standard for all calculations. In order to bracket uncertainties arising from uncertainty in the ozone profiles, all calculations were also performed with the ozone profiles from Fiji, and these results are shown where appropriate. The climatological mean data are used with the explicit consideration of the semiannual and annual cycles.

2.2. Radar Cloud Retrieval

[14] The radar reflectivity (Z_e) data from the MMCR are used to retrieve the following microphysical parameters to characterize the cloud profiles: ice water content (IWC), effective particle size (D_{ge}), snow/graupel water content (SWC), liquid water content (LWC), effective droplet size (r_e), and rain water content (RWC). For ice clouds ($dBZ_e \leq 10$), following *Liu and Illingworth* [2000], $IWC = 0.097\ Z_e^{0.59}$ where IWC is in gm^{-3} and Z_e is in $mm^6\ m^{-3}$. Using the in situ observed data shown by *Fu et al.* [1998], we have $D_{ge} = 192\ IWC^{0.331}$ where D_{ge} is in μm. For $10 < dBZ_e \leq 20$, we derive the SWC using the same equation as for ice, but a mean effective radius of 974 μm is used for snow/graupel particles [*Fu et al.*, 1995]. For water clouds ($dBZ_e \leq -7$), following *Sassen and Liao* [1996] $LWC = 6.34\ Z_e^{0.5\bar{5}\bar{6}}$ where LWC is in $g\ m^{-3}$. By assuming a lognormal size distribution with a number density of 100 cm^{-3} and a logarithmic width of 0.35, we derive $r_e = 15.1\ LWC^{1/3}$ where r_e is in μm. When $-7 < dBZ_e \leq 20$, we consider the Z_e is due to rain precipitation. Following *Frisch et al.* [1995] $RWC = 0.076 \cdot Z_e$ where RWC is in $g\ m^{-3}$. We assume that $r_e = 80\ \mu m$ for $-7 < dBZ_e \leq 10$ due to drizzle and $r_e = 488\ \mu m$ for $10 < dBZ_e \leq 20$ due to rain [*Fu et al.*, 1995]. In this work we do not consider the mixed-phase clouds. We assume that clouds and precipitation are ice phase when T (0°C and liquid phase when $T > 0$°C. No retrieval is performed when $dBZ_e > 20$. The limit where the radar reliably identifies clouds is at a condensate content of order 10^{-2} g/m^3 for liquid, and 10^{-3} g/m^3 for ice (T. Ackerman and R. Marchand, personal communication, 2006). Visual inspection of the results of the retrieval algorithm (see also Figure 6 below) show that this limit is too conservative, and dismisses echoes that are clearly cloudy. We thus push this limit to a lower detection limit of 10^{-4} g/m^3 (equivalent to about 0.6 ppmv in the condensed phase at $p = 150$ hPa/$T = 200$ K). Visual inspection shows that with this threshold the number of echoes classified as "cloudy" which are not associated with a larger cloud structure, and thus may be an artefact, is very small (see also Figure 6 below). Note that pushing the detection

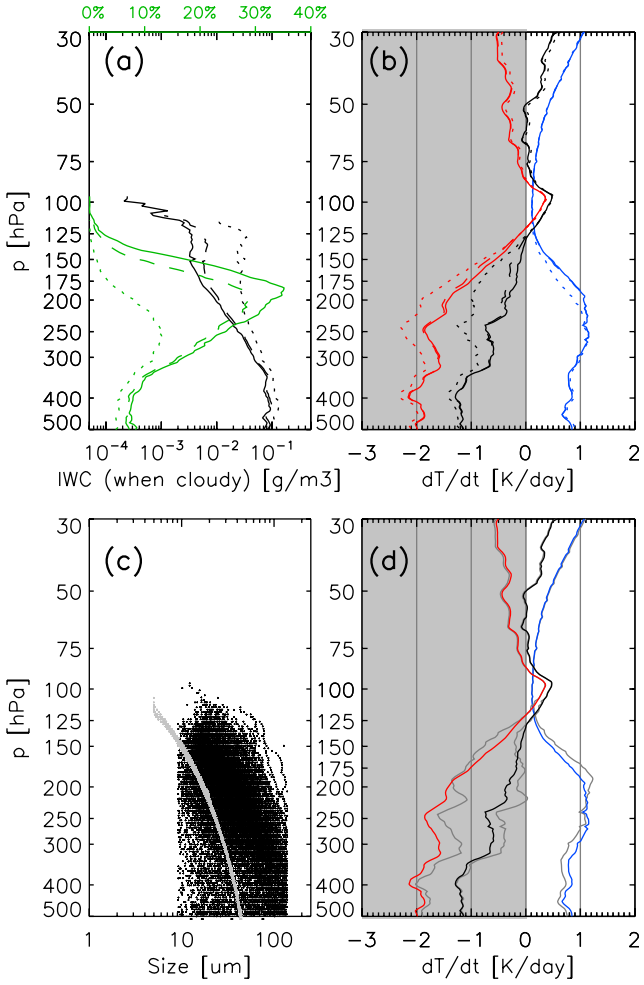

Figure 5. Sensitivity (a and b) to lower threshold for ice cloud detection (dotted/dashed/solid = 10^{-2}, 10^{-3}, 10^{-4} g/m^3) and (c and d) to parameterization of ice particle sizes, calculated for Manus, March 2000. Figure 5a shows average ice water content when cloudy (black lines) and ice occurrence frequency (green lines, in percent). Figure 5b shows corresponding radiative heating rates (red indicates longwave, blue indicates shortwave, and black indicates total). Figure 5c shows ice particle sizes determined from parameterization used here (black, based on IWC) and alternative parameterization (grey, based on temperature), with a detection threshold of 10^{-4} g/m^3). Figure 5d shows corresponding heating rates (colors indicate this work, and grey indicates alternative). See text for description of parameterizations.

limit to 10^{-4} g/m^3 only improves the detection results for thin clouds; it does not imply that the radar reliably detects clouds with such low ice content.

[15] Figure 5 shows results of sensitivity studies with respect to retrieval thresholds and ice particle size parameterizations. All calculations are based on the data from Manus for the period of March 2000 (a location and period where the radar was almost continuously in operation, and where frequently high clouds occurred). Figure 5a shows the average ice water content when the algorithm detects an ice cloud for a detection limit of 10^{-2}, 10^{-3}, 10^{-4} g/m^3, as well as the corresponding ice occurrence frequencies. Figure 5b shows the corresponding radiative heating rates. Figure 5 shows that results do depend on the choice of detection threshold, but are not overly sensitive as long as this limit is 10^{-3} g/m^3. As the true distribution of clouds with IWC 10^{-3} g/m^3 is not known, no statement can be deduced on the absolute accuracy of the radiative transfer calculations based on the cloud retrieval from the MMCR. We will further discuss this with additional sensitivity calculations in section 3.5.

[16] We further tested results using a retrieval with a parameterization of the size of the ice particles as function of temperature. On the basis of the data presented by *Boudala et al.* [2002] and *Garrett et al.* [2003], we obtain from a least square fit $D_{ge} = 47.05 + 0.6624 \times T + 0.001741 \times T^2$, where T is temperature in centigrade, for the temperature range [−80,0]°C. Figure 5c shows that the two different parameterizations yield a fairly different profile of D_{ge}, leading to differences in calculated heating rates (Figure 5d) mainly in the troposphere. In the lower stratosphere differences are small.

[17] Figure 6 shows an example of the radar backscatter data, the retrieved liquid/ice water content, and results of the radiative transfer calculations (discussed below). Note the repeated occurrence of deep convective clouds with rainfall at the cloud base, and more sporadic high cirrus clouds, either from convective outflow elsewhere or formed in situ.

[18] The ARM MMCR data provide a quality flag for each profile at each altitude (MMCR Mode Quality Control Flags). All profiles marked as "no significant power return" or "data do not exist" are discarded. However, profiles having minor problems at single levels (which affect the results only little) are kept, as we value it more important to have representative statistics (in time).

2.3. Radiative Transfer Calculations

[19] We calculate the radiative heating profiles with a radiative transfer model [*Fu and Liou*, 1993]. The radiative transfer scheme is based on the delta-four-stream approximation [*Liou et al.*, 1988; *Fu et al.*, 1997]. The correlated k-distribution method is used to treat the nongray gaseous absorption due to H_2O, CO_2, O_3, N_2O, and CH_4 [*Fu and Liou*, 1992]. The H_2O continuum absorption, CKD 2.4 [*Tobin et al.*, 1999] is used in the thermal spectra. The single-scattering properties of nonspherical ice particles are parameterized following *Fu* [1996] and *Fu et al.* [1998]. The single-scattering properties of water clouds, snow/graupel, and rain are based on the Mie calculations [*Fu et al.*, 1995].

[20] The surface albedo is set to 0.1 (typical for marine conditions), and all tracer concentrations are set to typical present-day values (CO_2: 365 ppmv; CH_4: 1.75 ppmv; N_2O:0.315 ppmv; CFC-11: 0.27 ppbv; CFC-12: 0.535 ppbv CFC-22: 0.105 ppbv). Solar insolation is calculated for the stations' latitudes, including diurnal and annual cycles.

[21] All heating rates are calculated for "clear sky," i.e., without considering clouds, and "all sky," i.e., with the cloud information. The difference between the all sky and the clear sky calculation yields the impact of the tropospheric cloud field on stratospheric heating rates (alternatively, one might see this also as the error in the calculated heating rates if clouds were neglected). Figure 6c shows the

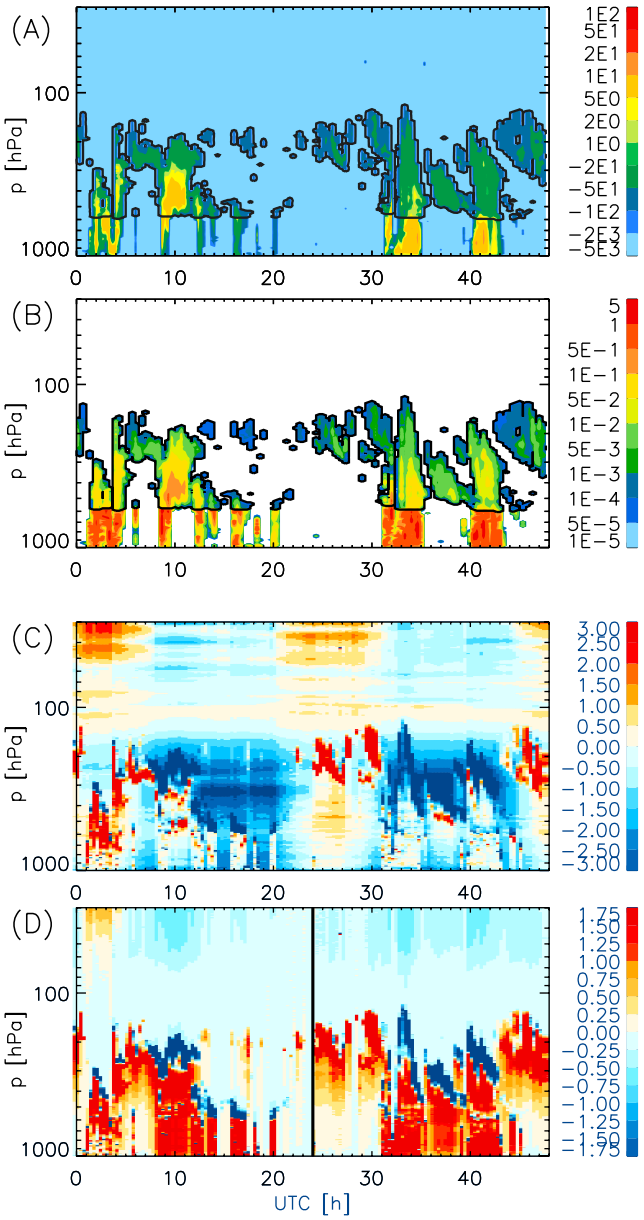

Figure 6. Episode (Manus, 22–23 June 2000) illustrating the processing sequence. (a) Radar signal (dBz) (black contours indicate ice clouds after retrieval); (b) cloud-radar retrieved condensed mass content (ice, graupel, liquid and rain) in g/m^3 (black contours around ice phase); (c) radiative heating rates (K/day, all sky calculation); and (d) radiative heating rate difference between all sky and clear sky calculation (K/day, note change of color scale). Profiles with invalid radar data (which are not used in this study, see text) are shown in black.

results of the all sky calculation for the exemplary episode. Figure 6d shows the difference between all sky and clear sky calculation. Several aspects of the impact of clouds can be seen in this 2-day episode. From about 0100 UTC to 0400 UTC (note that the shift to local time is about 10 hours for Manus), the midlevel clouds (cloud tops near 300 hPa) actually increase stratospheric heating rates above about 50 hPa. This is to be understood as the consequence of increased upwelling short wavelength radiative fluxes, but less reduced upwelling longwave radiative fluxes. Conversely, in the case of the higher clouds just before, and just after that period, the effect of the reduction in upwelling longwave exceeds that of the increased shortwave flux. Obviously, the strongest reduction in stratospheric heating rates occurs for the highest clouds during night time (e.g., around 1000 UTC).

[22] Note that the clouds fields even more strongly affect the tropospheric heating rates (Figures 6c and 6c), with similar day/night and vertical cloud structure effects. They are, however, not the subject of this paper and will not be further discussed here.

2.4. Data Processing

[23] Gas phase and condensed phase profiles are evaluated with a sampling period of 20 min (yielding 72 profiles per day), whereby each radar retrieval is based on the mean profile of three consecutive radar profiles with a sampling period of 10 s as provided by the ARM data distribution. The subsampling is performed in order to reduce the amount of data to be processed. For each profile the radiative heating rates are calculated, with (all sky) and without the condensed phase profile (clear sky). Although the valid radar profiles are quite evenly distributed over the course of day (see Figure 3), we first obtain an average radiative heating rate profile for each time of day (for given month) to avoid any bias arising from biases in diurnal sampling (some months have very variable number of valid profiles for given UTC).

[24] We thus obtain a monthly mean diurnal cycle of heating rates for each month with valid data. The average of this monthly mean diurnal cycle then yields the monthly mean radiative heating rate profiles (and similarly the monthly mean temperatures, tracers, and ice and liquid water contents). Note that the monthly mean impact of clouds is not the difference between the monthly mean all sky and clear sky profile, but the averaged difference (in the same fashion as described above) between the all sky and clear sky calculation of each individual profile.

3. Results

[25] We will first show some results of the cloud retrievals (section 3.1) to describe the cloud field structure and variability. Section 3.2 shows an estimate of the cloud effects on radiative heating rates using prototype clouds. Section 3.3 presents the results of the clear sky calculations, with an emphasis on wave-induced radiative heating rate variations. Section 3.4 shows the annual mean, seasonal variability of monthly mean, and monthly mean radiative heating rate profiles, as well as the impact of clouds on these profiles. Section 3.5 discusses the impact of thin cirrus which are not detected by the MMCR, and section 3.6 shows the seasonal variability of the level of zero net radiative heating.

3.1. Retrieved Cloud Fields

[26] Figure 7 shows the monthly mean ice occurrence frequency distribution at Manus and Nauru for all months when data are available. We note significant differences, with lowest ice occurrences for Nauru in 2000. Nauru in

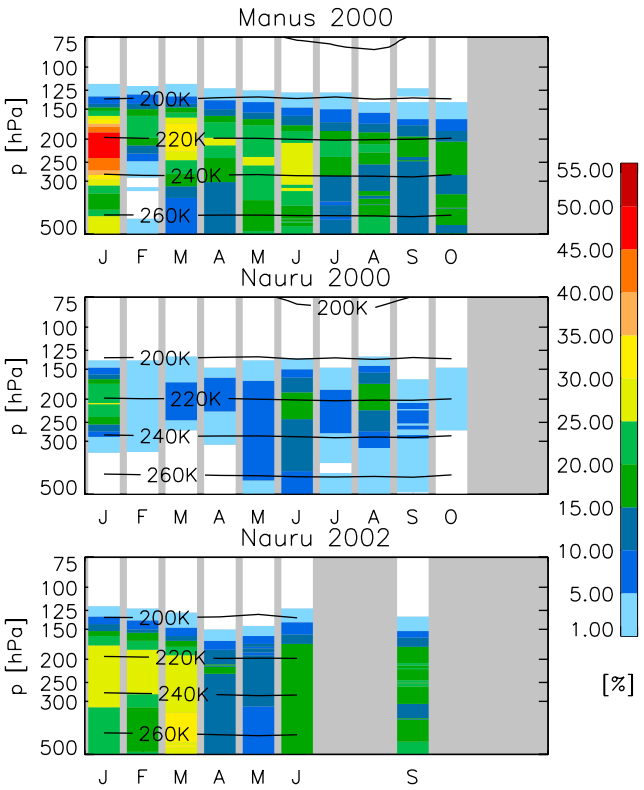

Figure 7. Monthly mean ice occurrence frequency (color scale, when valid data are available) for Manus 2000, Nauru 2000 and Nauru 2002. Black solid lines show monthly mean temperatures.

2002 shows increased ice occurrences compared to 2000, perhaps due to the developing El Nino situation in 2002 which is accompanied by an eastward shift of convective activity (the ENSO signal is weak in that period, however, and the difference may also reflect stochastic variability). We note that, even for months with relatively high radar data coverage (in time, see Figure 3), the number of deep convective events is typically between 1 and 10 per month (Figure 6 shows a sequence with above average convective cloud occurrence). Consequently, the statistics based on observations at a fixed location show large variability even for monthly mean values.

[27] Figure 7 further shows the monthly mean temperature profiles (dashed contour lines), which give an indication of the emission temperature of the cloud layer. On average, the highest clouds have a cloud top temperature around 200 K. Note, however, that the ice water content of these very high clouds is small, such that the average effective emission temperature will be dominated by lower, and hence warmer, cloud layers.

3.2. Idealized Calculations of the Impact of Clouds

[28] Figure 8 shows the impact of idealized cloud fields on lower stratospheric heating rates. The calculations assume diurnal mean solar insolation for equinox conditions, and the prototype clouds are inserted at different pressure levels (corresponding to different cloud top temperatures) with varying optical depths (achieved by varying the geometrical thickness of the clouds). As discussed previously, for very low (high temperature) cloud tops, the net effect is an increase in heating rates, whereas for higher clouds the net effect is a decrease (up to about 10–30 hPa, Figure 8b), depending also on optical depth of the cloud. Together with Figure 7 this allows an estimate of the order of magnitude expected of radiative heating rate changes due to clouds over Manus and Nauru. We note that in 2000 Manus, and in 2002 Nauru, have both frequent high clouds with cloud top temperatures in the range of 220 to 210 K, such that we may expect for these cases a reduction of radiative heating rates of order 0.1–0.2 K, whereas for Nauru in 2000, the effect may be a factor 2 or so smaller because of the smaller cloud occurrence frequency.

3.3. Clear Sky Radiative Heating Rates

[29] Figure 9 shows the diurnal mean clear sky radiative heating rates of the upper troposphere and lower stratosphere for two episodes (April-May, November-December) at Manus in 2000. Note that the rawinsonde data are available for the entire year, such that clear sky calculations can be performed for the full year, whereas the all sky calculations are limited by the availability of radar data. Figure 9 shows much lower heating rates in the lower stratosphere for April-May than for November-December. Figure 9 also shows much stronger variation in heating rates associated with temperature perturbations from Kelvin

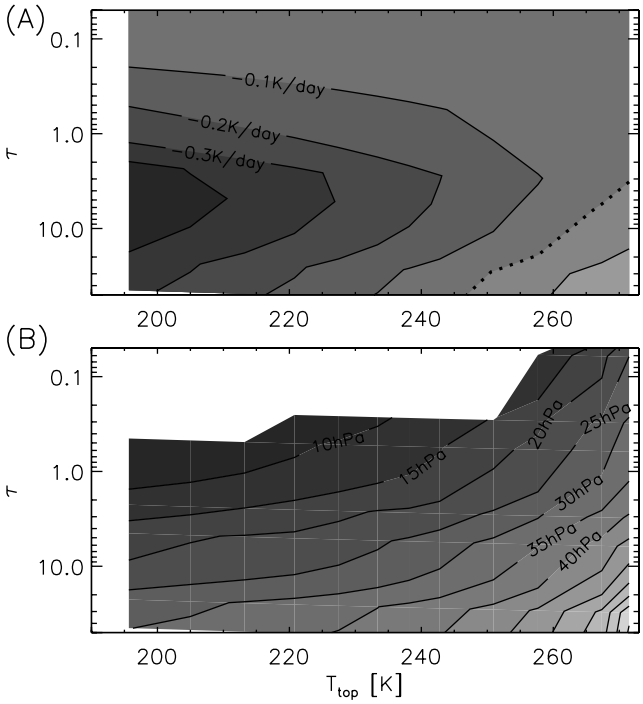

Figure 8. Radiative transfer calculations for idealized cloud fields with varying optical depth (y axis) and cloud top temperature (x axis). Calculations assume diurnal mean insolation. (a) Cloud impact on radiative heating rates for the layer 70–30 hPa. Dotted line indicates zero and the contour spacing is 0.1 K/day. (b) Pressure level where the total cloud radiative effect reverses sign (from reduced heating rates below that level to increased heating rates above that level). Contour spacing is 5 hPa, and white area indicates reversing level is above 5 hPa or nonexistent.

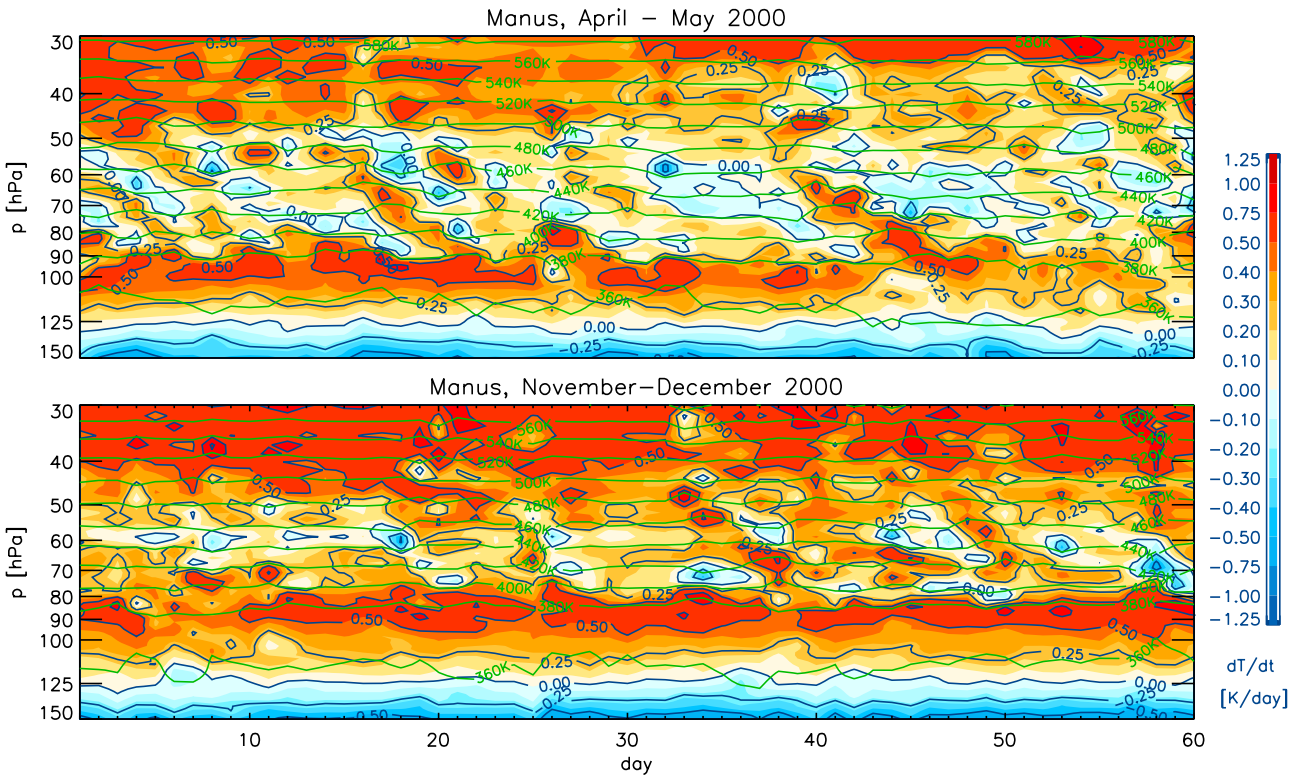

Figure 9. Diurnal mean clear sky radiative heating rates (color, note change in increments from 0.1 to 0.25 K/day at ±0.5 K/day; black labeled isolines with regular spacing of 0.25 K/day) with potential temperature isolines (green; as labeled, in Kelvin) for Manus for two 2-month periods ((top) April-May 2000 and (bottom) November-December 2000). Downward deflection of potential temperature isoline is caused by a positive (warm) temperature anomaly, which induces a negative heating rate anomaly. Note wave structures, presumably arising from Kelvin waves.

waves during April-May than November-December. We note that the period October-December shows a minimum in variability related to Kelvin waves for both Manus and Nauru.

[30] A detailed analysis of the Kelvin wave induced variability of lower stratospheric heating rates is beyond the scope of this paper, and will be discussed elsewhere. We note, however, that the heating rate modulations due to Kelvin waves are substantial (of order 1 K/day), lasting typically for a few days. In addition to these transient temperature perturbations, the Kelvin wave induced temperature (and hence also radiative heating rate) variations show quasi-stationary patterns [*Randel and Wu*, 2005], and both could have an impact on transport and mixing in the tropical lower stratosphere.

3.4. Radiative Heating Rates in the TTL and Lower Stratosphere

[31] Figures 10 and 11 show the annual mean and seasonal variability of the radiative heating rates for Manus and Nauru in 2000, where we used a fit (for each level) with harmonics of period 12 months (to capture the annual cycle) and 6 months (to allow for some variation on a semiannual timescale) in order to obtain an objective annual mean despite lack of data for 2 consecutive months. The same procedure was not applied to Nauru 2002 (with 4 months of missing data), and for this case we present the results for the individual months only (see below). Figures 10a and 11a show the annual mean radiative heating rate of the all sky calculation using the ozone data from Java (solid, standard case) and Fiji (dashed). The heating rates show a transition from cooling in the troposphere to heating at p $\sim$ 130 hPa (about 355 K in potential temperature), a pronounced maximum near the tropopause, and a local minimum around 70–60 hPa (about 435 K potential temperature), with increasing values higher up. The generally higher ozone values of Fiji result in an increase in the calculated heating rates of about 0.05 K/day throughout the profile. Figures 10c and 11c show the radiative heating rates for January (blue), April (green), July (red) and October (olive) 2000 of the all sky calculation using the standard ozone profiles. The radiative heating rates show a pronounced seasonality, which follows to first order that of the layer temperature, but is also modulated by the variations in temperatures of adjacent layers as well as cloud cover. Sensitivity calculations (not shown) with (1) ozone mixing ratios and (2) both ozone and tropospheric water vapor mixing ratios held constant, show that these factors play only a secondary role for the seasonal variability of radiative heating rates in the tropical lower stratosphere.

[32] The difference between the all sky calculations and the clear sky calculations ($\delta(\partial T/\partial t)$) on an annual mean basis is shown in Figures 10b and 11b. The lower stratospheric heating rates of the all sky calculations are about

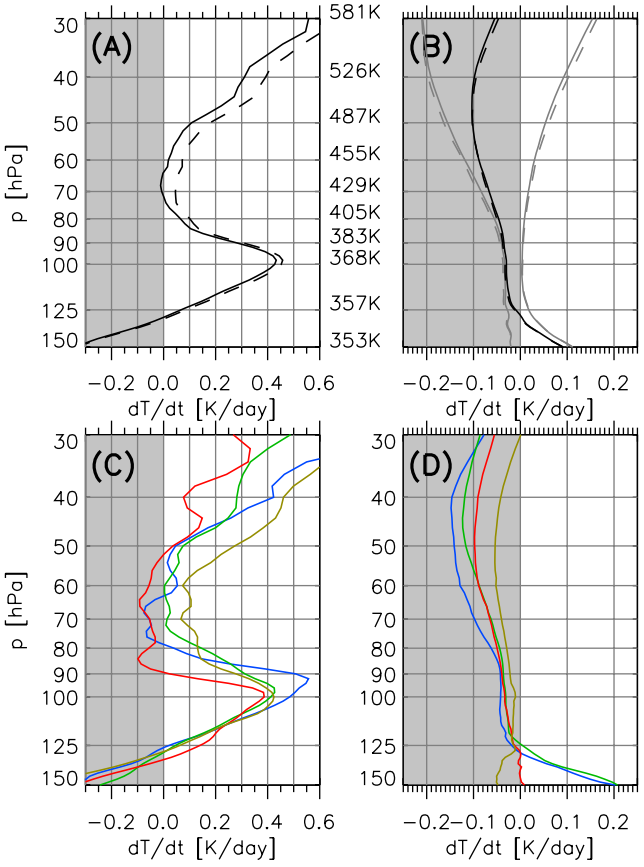

Figure 10. Radiative heating rates for Manus, 2000. (a) Annual mean (calculations with ozone from Java (solid) and Fiji (dashed)); (b) difference between all sky and clear sky (black), for both ozone profiles, and separated into longwave and shortwave (grey). Potential temperature of pressure levels, based on annual mean temperature, as indicated. (c) All sky radiative heating rate profiles based on fits (see text) for January (blue), April (green), July (red) and October (olive). (d) Same as Figure 10c but for difference between all sky and clear sky calculation. No potential temperature of pressure levels is given because of its seasonality.

0.1 K/day (Manus 2000) and 0.05 K/day (Nauru 2000) smaller than those of the clear sky calculations. The larger reduction at Manus is due to the more frequent cloud occurrences over Manus than Nauru in 2000 (recall Figure 7). Figures 10b and 11b further show that the impact of the clouds on longwave and shortwave heating rates (grey lines) is of opposing sign. The reduction of the stratospheric heating rates due to clouds is only weakly sensitive to the ozone profile (solid grey vs. dashed grey lines), such that the quantification of the effect of clouds on heating rates is not affected by uncertainties in the ozone profile. Figures 10d and 11d show the total (shortwave and longwave) difference in the heating rates (all sky minus clear sky calculation) for January (blue), April (green), July (red) and October (olive). As expected, the effect is largest for months with most frequent high, thick clouds.

[33] Figure 12 shows the monthly mean effect of clouds on radiative heating rates for each month with available data (i.e., no fit is performed). Figure 12 shows even more pronounced correspondence to the tropospheric cloud field statistics (compare with Figure 7). These calculations based on a highly detailed description of the tropospheric cloud field show that in all cases the net effect of clouds is a reduction of heating rates in the lower stratosphere, with monthly mean maximum values of $\delta\,(\partial T/\partial t) \approx -0.2$ K/day. In cases of sparse high cloud coverage, e.g., Nauru in February-April 2000, the net effect in this layer is very small, and the effect of increased reflected shortwave flux dominates the response already from about 40 hPa (about 525 K) upward, whereas in most cases the reduction in radiative heating rates due to reduced upwelling longwave radiation dominates up to about 30 hPa (about 600 K).

3.5. Impact of Thin Cirrus

[34] Thin cirrus in the upper troposphere may go undetected by the radar system (as discussed before) but can have an impact on the radiative fluxes particularly when situated close to tropopause levels. In principle the ARM program operates ground-based lidar systems in Manus and Nauru for the detection of such clouds. *Comstock et al.* [2002] showed that the lidar system detects higher cloud tops than the MMCR. However, the times when both lidar and radar system operate simultaneously are too sparse in the selected period to allow reliable estimates of seasonal variability. Further, the lidar is plagued with problems in the presence of thick tropospheric clouds. We have therefore chosen to conduct this study with the radar data only, but to

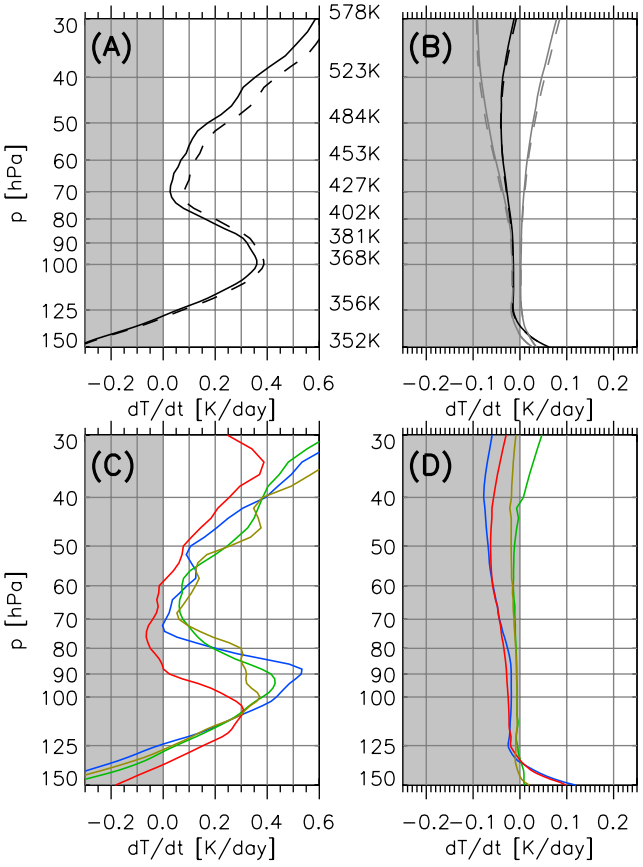

Figure 11. (a–d) Same as Figure 10 but for Nauru, 2000.

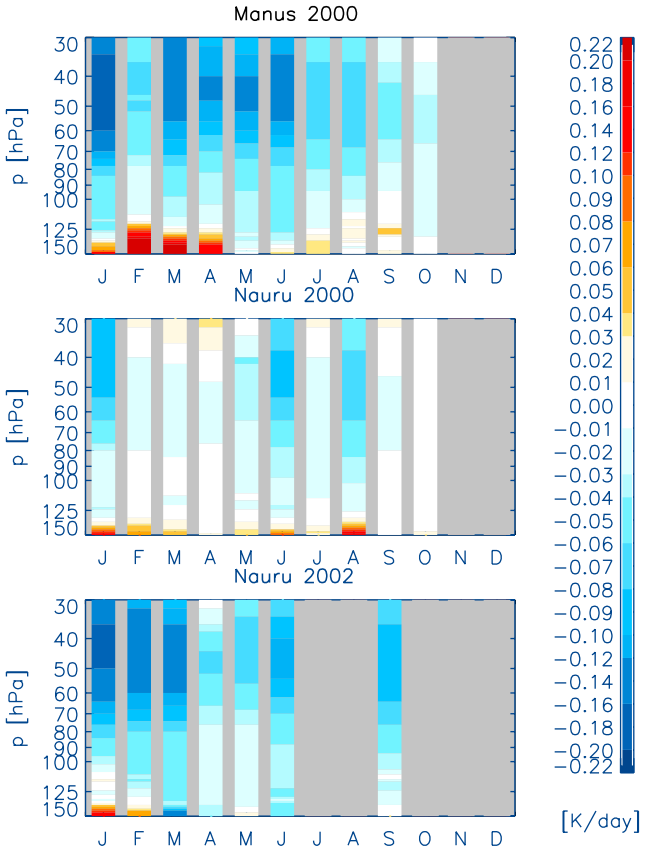

Figure 12. Monthly mean difference of all sky minus clear sky radiative heating rates (δ ($\partial T/\partial t$), in K/day) for all months used in this study.

bracket the impact of thin cirrus clouds by inserting thin prototype clouds near the tropopause into the retrieved cloud fields.

[35] Figure 13 shows the impact of inclusion of thin cirrus clouds on lower stratospheric heating rates. The radiative heating rates are calculated for different "prototype" thin cirrus clouds with optical depths of τ = 0.005, 0.015 and 0.03, i.e., "subvisible" clouds according to *Sassen and Cho* [1992]. The clouds are inserted between 108 and 100 hPa, corresponding to a geometric thickness of about 550 m. The radiative effect of these clouds depends on particle size, and we present calculations for D_{ge} = 10 and 15 μm (yielding a total of 6 different clouds). The calculations were also done for the same set of clouds, but inserted between 102 and 95 hPa (i.e., very close to the cold point tropopause). The results were very similar and therefore not discussed below.

[36] Figure 1 shows the results for the calculations using the cloud fields observed over Manus in 2000. The additional reduction of radiative heating in the lower stratosphere due to these thin cirrus clouds is of order −0.005 to −0.02 K/day (depending on optical depth and particle size), about an order of magnitude smaller than that resulting from the cloud field as retrieved from the MMCR data. Observed occurrence frequencies of thin cirrus clouds near the tropical tropopause show maxima of 50–70% over heavy convective regions (continents, maritime continent, western Pacific; depending on season) [e.g., *Wang et al.*, 1996; *Spang et al.*, 2002]. Thus their impact may be even smaller than in these calculations, which supports our earlier assertion that they play only a secondary role for the radiative heating rates in the lower stratosphere. These results are also consistent with those of *Corti et al.* [2005], showing differences of tropical mean radiative heating rates around 20 km for the period 10–19 September 1994 of order 0.01 K/day between calculations using only the ISCCP database and those where they included thin cirrus clouds as retrieved from LITE. The month to month variability of the impact of a given cloud prototype seen in Figure 13 is small (only February 2000 shows a larger deviation), which implies that the modulation of the impact by the underlying cloud field is small. In fact, the net effect of thin cirrus for which we use radar cloud information differs not so much from the effect calculated when the tropospheric cloud field was ignored altogether (not shown). Finally, we note that the calculations assuming smaller particles yield a smaller reduction of lower stratospheric heating rates because of their larger cloud albedo (which increases the positive short wavelength effect) and smaller long wave emissivity (which decreases the negative long wavelength effect).

[37] These calculations further allow us to assess the likelihood of the process suggested by *Hartmann et al.* [2001b], namely that thin cirrus above thick anvil clouds could lead to substantial radiative cooling around tropopause levels. Figure 14 shows the histograms of changes of radiative heating in the thin cirrus cloud layer itself (again for Manus 2000). The statistics shown in Figure 14 suggest that the cases where cooling results are very rare compared to those where heating results. Assuming 100% cloud occurrence frequency may artificially skew the histograms. For example, one may hypothesize that in reality, the clouds may be present predominantly in those cases where a cooling effect prevails. However, their high occurrence frequency of 50–70% mentioned above renders it impossible to significantly shift the histograms as shown in

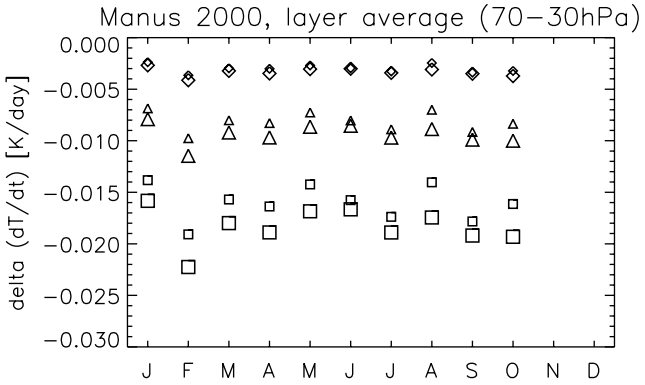

Figure 13. Change of layer-mean radiative heating between 70 and 30 hPa due to thin cirrus near the tropopause. Calculations assuming thin cirrus between 108 and 100 hPa (550 m thick) with 100% occurrence frequency above cloud fields retrieved from MMCR over Manus in 2000, compared to calculation based on MMCR cloud field only. Results shown for thin cirrus with optical depths τ = 0.005 (diamonds), τ = 0.015 (triangles) and τ = 0.03 (squares). Assumed effective particle size D_{ge} = 10 μm (small symbols) and 15 μm (large symbols).

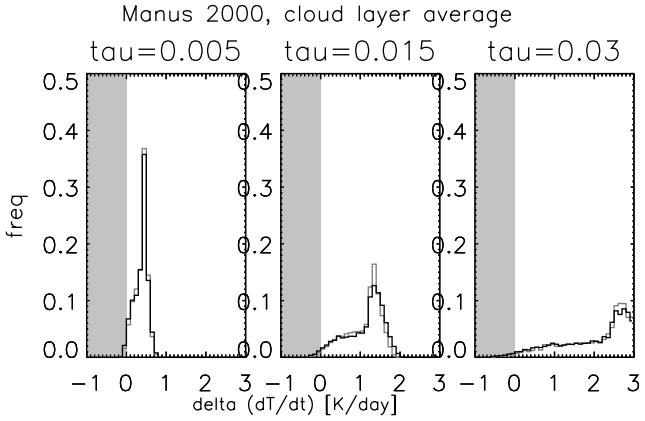

Figure 14. Histograms of change in radiative heating rate in tropopause thin cirrus clouds with optical depths (left) τ = 0.005, (middle) 0.015 and (right) 0.03 with effective particle sizes D_{eg} = 10 μm (black) and 15 μm (grey). (Same calculations as for Figure 13.)

Figure 14. It thus appears unlikely that thin cirrus clouds could account for the required "energy sink" to explain the results of *Sherwood* [2000].

3.6. Level of Zero Net Radiative Heating

[38] The level of zero net radiative heating has recently come into focus as a potentially important level [e.g., *Gettelman et al.*, 2004], marking the transition from the moist convectively driven tropospheric Hadley circulation to the wave-driven stratospheric circulation, and has been proposed as a definition for the bottom of the tropical tropopause layer [*Sherwood and Dessler*, 2000]. As pointed out previously, the radar-based cloud retrieval is biased toward underestimating very high, thin cirrus. These clouds have an impact on the heating rates in the TTL [e.g., *Corti et al.*, 2005] (see also previous section), and consequently on the location of the level of net zero radiative heating. Using the radar-based cloud properties allows to determine that level in the presence of clouds, but must be regarded only as a first step of improvement compared to clear sky calculations or calculations using idealized cloud fields [e.g., *Gettelman et al.*, 2004].

[39] Figure 15 shows that the calculations based on clear sky and all sky in fact yield very similar results for the level of zero radiative heating. That is, in the cloud field as resolved by MMCR the strong radiative heating and cooling of individual clouds (recall Figure 6) largely cancels at these altitudes. The level is found at about a potential temperature of 355–360 K (15 km), with some seasonal variability of 3–4 K (400–500 m), similar to the results based on clear sky calculations presented by *Gettelman et al.* [2004]. The all sky calculations yield levels that are typically about 100 m lower than those in the clear sky calculations. The results of equatorial (10°S–10°N), zonal mean radiative heating rates shown by *Corti et al.* [2005] suggest a lowering of the level of net zero radiative heating of about 1 km when including the ISCCP cloud field (which might overestimate the thin cirrus effects), almost a factor 10 larger than our estimate. Replacing the ISCCP thin cirrus and cloud top information by those retrieved from LITE reduced their lowering to about 500 m.

[40] The level of zero net radiative heating is also sensitive to water vapor concentrations in the upper troposphere, which may have a low bias as discussed in section 2.1. The sensitivity experiment with 20% increased water vapor mixing ratios between 300 and 100 hPa shows that, in the monthly mean, the level rises in height by about 100 m in the clear sky calculations, and about 50 m in the all sky calculations.

4. Summary and Discussion

[41] The radiative transfer calculations using the tropospheric cloud field as derived from ground-based millimeter radar over two sites in the western tropical Pacific show that the clouds can substantially reduce lower stratospheric radiative heating rates compared to clear sky calculations by δ ($\partial T/\partial t$) $\approx$ −0.2 K/day for periods of high cloud occurrence frequency. This number is large when compared to the absolute clear sky radiative heating rates in that layer, particularly around about 70–60 hPa (435–475 K potential temperature) where there is a local minimum, with clear sky heating rates of order $\partial T/\partial t$ = 0.2 K/day. There is some discussion in the literature whether such a minimum is real [*Eluszkiewicz et al.*, 1997]. Our calculations clearly support its existence, the question remaining, though, is its absolute value. The heating rates in this layer are sensitive to ozone concentrations, and the lack of ozone profiles at the two stations Manus and Nauru introduces an uncertainty in the calculation of absolute heating rates of order 0.1 K/day throughout the lower stratosphere (i.e., they shift the profiles, but do not alter their shape). Notwithstanding, it thus

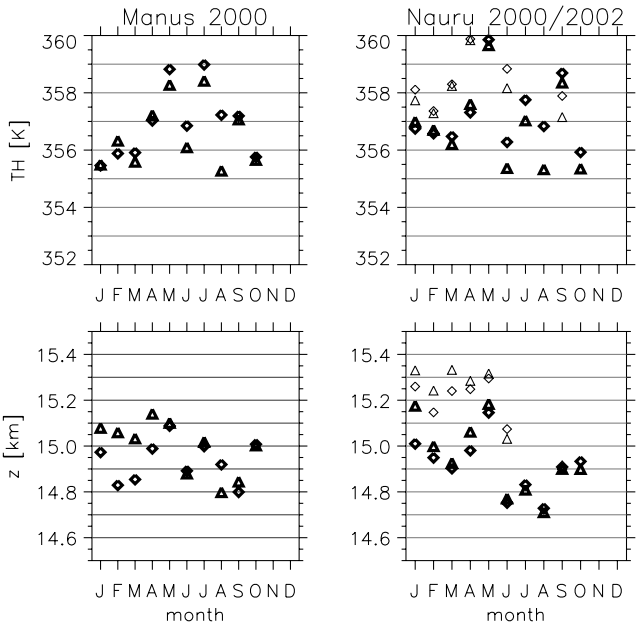

Figure 15. Level of net zero radiative heating in (top) potential temperature and (bottom) geometric height for (left) Manus in 2000 and (right) Nauru in 2000 and 2002. Triangles indicate clear sky calculations. Diamonds indicate all sky calculations using cloud field retrieved from MMCR data. Open symbols are for Nauru 2002.

appears that lower stratospheric radiative heating rates over heavily convective areas are very small, and may even be negative at times (i.e., air is diabatically descending).

[42] Differential diabatic heating can lead to mixing, a process which has been hitherto discussed primarily in the context of meridional gradients in stratospheric radiative heating rates [e.g., *Sparling et al.*, 1997]. The persistent spatial structures of tropical high cloud coverage on seasonal timescales lead to spatial structure in stratospheric radiative heating rates, and hence to mixing. Further, the radiative heating rate variations arising from transient and quasi-stationary temperature perturbations from Kelvin waves may also affect vertical mixing.

[43] The calculations shown here are based on a cloud retrieval using MMCR data that misses some thin cirrus clouds. Visual inspection of retrieval results shows that the detection threshold can be pushed to a condensate concentration of 10^{-4} g/m^3, however, this does not imply that the radar reliably detects clouds with such low condensate content. The threshold for reliable detection may be about a factor 2 or so higher (i.e., 5×10^{-4} g/m^3, equivalent to about 1 ppmv in the condensed phase at p = 150 hPa/T = 200 K). We have tried to bracket the uncertainty arising from undetected clouds by adding prototype thin cirrus clouds into the profiles, and comparing the results of the radiative transfer calculations with those based on the MMCR cloud field. We find that the occurrence of thin cirrus near the tropopause additionally reduces lower stratospheric heating rates. Hence the calculations based on the MMCR cloud field provide a lower limit of the effect of clouds on stratospheric heating rates. However, the effect (an additional -0.005 to -0.02 K/day, depending on optical depth and ice particle size) is roughly an order of magnitude smaller than that of optically thick cumulonimbus or anvil cirrus clouds (which are reliably detected), and hence may play only a secondary role for the radiative heating rates of the tropical lower stratosphere. We have used these calculations further to estimate the role of these thin cirrus clouds for the radiative heating rates within the cloud layer. We find, in accordance with previous studies, that they are important for the radiative heating within the cloud layer. Our results, for a region of frequent high anvil cloud occurrence, show that in most cases the thin cirrus clouds induce radiative heating within them, and only in few cases the thin cirrus results in a reduction of heating rates. These results are based on the assumption of 100% cloud occurrence frequency (of the prototype thin cirrus clouds), but the statistics are so overwhelmingly skewed toward a net heating, that even a peculiar correlation between underlying cloud cover and thin cirrus is not expected to substantially modify this result.

[44] To summarize, the results shown here suggest that the effect of clouds on tropical lower stratospheric radiative heating rates is important to understand the spatial structure of diabatic heating rates, but is insufficient to explain the magnitude of variability reported elsewhere [*Sherwood*, 2000; *Norton*, 2001; *Fueglistaler et al.*, 2004].

5. Outlook

[45] The spatial structure of high cloud occurrence frequency could imply a zonal residual circulation superimposed on the lower stratospheric mean meridional circulation as previously suggested (but substantially smaller in magnitude because of a different physical process) [*Gage et al.*, 1991; *Sherwood*, 2000]. It remains to be seen whether, e.g., atmospheric tracer observations can provide additional constraints on such a circulation, and whether variations related to El Nino/Southern Oscillation (leading to spatial redistribution of convection) can be detected. An accurate calculation of tropical mean diabatic heating rates at the local minimum of heating rates around 80–50 hPa (corresponding to about 410–480 K potential temperature) may provide further insight into the circulation of the stratosphere, and the transition from the lower stratosphere (with net divergence out of the tropics) to the "tropical pipe" [*Plumb*, 1996] region. Further, the strong anomalies of diabatic heating in the tropical lower stratosphere reported in the literature require further attention. The fact that meteorological analyses seem to capture at least some of these anomalies suggests that a detailed analysis of the energy budget of these models, and the role of the assimilation process, might shed further light onto the mechanisms.

[46] **Acknowledgments.** Data were obtained from the Atmospheric Radiation Measurement (ARM) Program sponsored by the U.S. Department of Energy, Office of Science, Office of Biological and Environmental Research, Environmental Sciences Division. We thank S. Hollars for preparing the temperature and water vapor profiles of Manus and Nauru. We thank the SHADOZ program for providing the ozone measurements. We thank MeteoSwiss for providing access to ECMWF operational analysis data. S.F. has been supported by NASA grants NNG04GM23G and 6524 Aura/HIRDLS.

References

Boudala, F. S., G. A. Isaac, Q. Fu, and S. G. Cober (2002), Parameterization of effective ice particle size for high latitude clouds, *Int. J. Climatol.*, *22*(10), 1267–1284.

Comstock, J. M., T. P. Ackerman, and G. G. Mace (2002), Ground-based lidar and radar remote sensing of tropical cirrus clouds at Nauru Island: Cloud statistics and radiative impacts, *J. Geophys. Res.*, *107*(D23), 4714, doi:10.1029/2002JD002203.

Corti, T., B. P. Luo, T. Peter, H. Vmel, and Q. Fu (2005), Mean radiative energy balance and vertical mass fluxes in the equatorial upper troposphere and lower stratosphere, *Geophys. Res. Lett.*, *32*, L06802, doi:10.1029/2004GL021889.

Doherty, G. M., R. E. Newell, and E. F. Danielsen (1984), Radiative heating rates near the stratospheric fountain, *J. Geophys. Res.*, *89*(D1), 1380–1384.

Eluszkiewicz, J. E., D. Crisp, R. G. Grainger, A. Lambert, A. E. Roche, J. B. Kumer, and J. L. Mergenthaler (1997), Sensitivity of the residual circulation diagnosed from the UARS data to the uncertainties in the input fields and to the inclusion of clouds, *J. Atmos. Sci.*, *54*, 1739–1757.

Frisch, A. S., C. W. Fairall, and J. B. Snider (1995), Measurement of stratus cloud and drizzle parameters in ASTEX with a Ka-band Doppler radar and a microwave radiometer, *J. Atmos. Sci.*, *52*(16), 2788–2799.

Fu, Q. (1996), An accurate parameterization of the solar radiative properties of cirrus clouds for climate models, *J. Clim.*, *9*, 2058–2082.

Fu, Q., and K. N. Liou (1992), On the correlated K-distribution method for radiative-transfer in nonhomogeneous atmospheres, *J. Atmos. Sci.*, *49*(22), 2139–2156.

Fu, Q., and K. N. Liou (1993), Parameterization of the radiative properties of cirrus clouds, *J. Atmos. Sci.*, *50*, 2008–2025.

Fu, Q., S. K. Krueger, and K. N. Liou (1995), Interactions between radiation and convection in simulated tropical cloud clusters, *J. Atmos. Sci.*, *52*, 1310–1328.

Fu, Q., K. N. Liou, M. C. Cribb, T. P. Charlock, and A. Grossman (1997), Multiple scattering parameterization in thermal infrared radiative transfer, *J. Atmos. Sci.*, *54*, 2799–2812.

Fu, Q., P. Yang, and W. B. Sun (1998), An accurate parameterization of the infrared radiative properties of cirrus clouds for climate models, *J. Clim.*, *11*(9), 2223–2237.

Fueglistaler, S., H. Wernli, and T. Peter (2004), Tropical troposphere-to-stratosphere transport inferred from trajectory calculations, *J. Geophys. Res.*, *109*, D03108, doi:10.1029/2003JD004069.

Gage, K. S., J. R. McAfee, D. A. Carter, W. L. Ecklund, A. C. Riddle, G. C. Reid, and B. B. Balsley (1991), Long-term mean vertical motion over the tropical Pacific: Wind-profiling Doppler radar measurements, *Science*, *254*, 1771–1773.

Garrett, T. J., H. Gerber, D. G. Baumgardner, C. H. Twohy, and E. M. Weinstock (2003), Small, highly reflective ice crystals in low-latitude cirrus, *Geophys. Res. Lett.*, *30*(21), 2132, doi:10.1029/2003GL018153.

Gettelman, A., J. R. Holton, and A. R. Douglass (2000), Simulations of water vapor in the lower stratosphere and upper troposphere, *J. Geophys. Res.*, *105*(D7), 9003–9023.

Gettelman, A., P. M. de F. Forster, M. Fujiwara, Q. Fu, H. Vmel, L. K. Gohar, C. Johanson, and M. Ammerman (2004), Radiation balance of the tropical tropopause layer, *J. Geophys. Res.*, *109*, D07103, doi:10.1029/2003JD004190.

Hartmann, D., L. A. Moy, and Q. Fu (2001a), Tropical convection and the energy balance at the top of the atmosphere, *J. Clim.*, *14*, 4495–4511.

Hartmann, D. L., J. R. Holton, and Q. Fu (2001b), The heat balance of the tropical tropopause, cirrus, and stratospheric dehydration, *Geophys. Res. Lett.*, *28*, 1969–1972.

Hicke, J., and A. Tuck (1999), Tropospheric clouds and lower stratospheric heating rates: Results from late winter In the Southern Hemisphere, *J. Geophys. Res.*, *104*(D8), 9309–9324.

Holton, J. R., P. H. Haynes, M. E. McIntyre, A. R. Douglass, R. B. Rood, and L. Pfister (1995), Stratosphere-troposphere exchange, *Rev. Geophys*, *33*, 403–440.

Liou, K. N., Q. Fu, and T. P. Ackermann (1988), A simple formulation of the delta-4-stream approximation for radiative-transfer parameterizations, *J. Atmos. Sci.*, *45*(13), 1940–1947.

Liu, C. L., and A. J. Illingworth (2000), Toward more accurate retrievals of ice water content from radar measurements of clouds, *J. Appl. Meteorol.*, *39*(7), 1130–1146.

Miloshevich, L. M., A. Paukkunen, H. Vömel, and S. J. Oltmans (2004), Development and validation of a time-lag correction for Vaisala radiosonde humidity measurements, *J. Atmos. Oceanic Technol.*, *21*(9), 1305–1327.

Moran, K. P., B. E. Martner, M. J. Post, R. A. Krofli, D. C. Welsh, and K. B. Widener (1998), An unattended cloud-profiling radar for use in climate research, *Bull. Am. Meteorol. Soc.*, *79*, 443–455.

Norton, W. A. (2001), Longwave heating of the tropical lower stratosphere, *Geophys. Res. Lett.*, *28*(19), 3653–3656.

Plumb, R. A. (1996), A "tropical pipe" model of stratospheric transport, *J. Geophys. Res.*, *101*(D2), 3957–3972.

Plumb, R. A., and J. Eluszkiewicz (1999), The Brewer-Dobson circulation: Dynamics of the tropical upwelling, *J. Atmos. Sci.*, *56*, 868–890.

Randel, W. J., and F. Wu (2005), Kelvin wave variability near the equatorial tropopause observed in GPS radio occultation measurements, *J. Geophys. Res.*, *110*, D03102, doi:10.1029/2004JD005006.

Rosenlof, K. H. (1995), Seasonal cycle of the residual mean meridional circulation in the stratosphere, *J. Geophys. Res.*, *100*(D3), 5173–5191.

Sassen, K., and B. S. Cho (1992), Subvisual-thin cirrus clouds lidar data set for satellite verification and climatological research, *J. Appl. Meteorol.*, *31*, 1275–1285.

Sassen, K., and L. Liao (1996), Estimation of cloud content by W-band radar, *J. Appl. Meteorol.*, *35*(6), 932–938.

Sherwood, S. C. (2000), A stratospheric "drain" over the maritime continent, *Geophys. Res. Lett.*, *27*, 677–680.

Sherwood, S. C., and A. E. Dessler (2000), On the control of stratospheric humidity, *Geophys. Res. Lett.*, *27*, 2513–2516.

Simmons, A. J., and J. K. Gibson (2000), The ERA-40 project plan, *ERA-40 Proj. Rep. Ser., 1*, 63 pp., Eur. Cent. for Med.-Range Weather Forecasts, Reading, U. K.

Simmons, A. J., A. Untch, C. Jakob, P. Kallberg, and P. Unden (1999), Stratospheric water vapour and tropical tropopause temperatures in ECMWF analyses and multi-year simulations, *Q. J. R. Meteorol. Soc.*, *125*, 353–386.

Spang, R., G. Eidmann, M. Riese, D. Offermann, P. Preusse, L. Pfister, and P. Wang (2002), CRISTA observations of cirrus clouds around the tropopause, *J. Geophys. Res.*, *107*(D23), 8174, doi:10.1029/2001JD000698.

Sparling, L. C., J. A. Kettleborough, P. H. Haynes, M. E. McIntyre, J. E. Rosenfield, M. R. Schoeberl, and P. A. Newman (1997), Diabatic cross-isentropic dispersion in the lower stratosphere, *J. Geophys. Res.*, *102*(D22), 25,817–25,830.

Thompson, A. M., et al. (2003), Southern Hemisphere Additional Ozonesondes (SHADOZ) 1998–2000 tropical ozone climatology: 1. Comparison with Total Ozone Mapping Spectrometer (TOMS) and ground-based measurements, *J. Geophys. Res.*, *108*(D2), 8238, doi:10.1029/2001JD000967.

Tobin, D. C., et al. (1999), Downwelling spectral radiance observations at the SHEBA ice station: Water vapor continuum measurements from 17 to 26 μm, *J. Geophys. Res.*, *104*(D2), 2081–2092.

Wang, J., D. J. Carlson, D. B. Parsons, T. F. Hock, D. Lauritsen, H. L. Cole, K. Beierle, and E. Chamberlain (2003), Performance of operational radiosonde humidity sensors in direct comparison with a chilled mirror dew-point hygrometer and its climate implication, *Geophys. Res. Lett.*, *30*(16), 1860, doi:10.1029/2003GL016985.

Wang, P. H., P. Minnis, M. P. McCormick, G. S. Kent, and K. S. Skeens (1996), A 6-year climatology of cloud occurrence frequency from SAGE II extinction measurements (1985–1990), *J. Geophys. Res.*, *101*, 29,407–29,429.

Q. Fu and S. Fueglistaler, Department of Atmospheric Sciences, University of Washington, Seattle, WA 98195, USA. (stefan@atmos.washington.edu)